

Doping-induced evolution of the intrinsic hump and dip energies dependent on the sample fabrication conditions in $\text{Bi}_2\text{Sr}_2\text{CaCu}_2\text{O}_{8+\delta}$

Tatsuya Honma

Department of Physics, Asahikawa Medical University
Asahikawa, Hokkaido 078-8510, Japan
honma@asahikawa-med.ac.jp

Abstract

In oxygen-doped $\text{Bi}_2\text{Sr}_2\text{CaCu}_2\text{O}_{8+\delta}$, the spectra, as observed by tunneling spectroscopy or photoemission measurements, depend on the sample fabrication conditions, such as the temperature and pressure for fabricating the junction or surface. This implies that the hump and dip energies extracted from the spectra depend on the sample fabrication conditions. When the samples were fabricated at 4.2 K and/or under ultrahigh vacuum (UHV), the hump energy exhibited a step-like doping dependence and the dip energy followed the upper pseudo-gap line. As the fabrication conditions deteriorated, the hump and dip energies reproduced the previous results, in that the dip energy was significantly dependent on the sample, whereas the hump energy exhibited a smooth hump doping dependence. It can be concluded that the observations for the samples fabricated at 4.2 K and/or under

UHV reflect the intrinsic bulk properties, whereas those for the samples fabricated under deteriorated conditions reflect degraded surface properties.

Keywords: high-temperature cuprate superconductor, electronic phase diagram, tunneling spectroscopy, photoemission, sample fabrication conditions.

1. Introduction

One of the characteristic features of high-temperature cuprate superconductors (HTCS) is the so-called peak-dip-hump (PDH) structure, which can be observed in the energy distribution curve (EDC) by angle-resolved photoemission spectroscopy (ARPES).¹ The peak, dip, and hump structures appear away from the Fermi level (E_F) in the order. A similar PDH structure can also be observed in the spectrum below E_F by superconductor-insulator-normal metal (SIN) tunneling spectroscopy.² However, the spectra were not symmetrical with respect to E_F . The dip and hump structures above E_F are sample dependent.³⁻⁸ In contrast, the spectra obtained by superconductor-insulator-superconductor (SIS) tunneling spectroscopy have a symmetrical PDH structure with respect to E_F .^{6,9-12} Despite the different experimental probes, the peak and hump energies followed the lower pseudo-gap (PG) and smooth hump lines in the unified electronic phase diagram (UEPD), respectively.¹³ The peak and hump energies are defined as the visible peak positions of the peak and hump structures, respectively. However, the dip energy did not follow any line in UEPD. The dip energy is roughly defined as the visible bottom position.

According to Giaever,¹⁴ the peak structure of the SIS tunneling spectrum can be well explained by a ‘peak-to-peak’ tunneling process. Furthermore, both the

symmetrical PDH structure in the SIS tunneling spectrum and the asymmetrical PDH structure in the SIN tunneling spectrum can be explained in terms of two tunneling processes, ‘hump-to-peak’ (Fig. 1(b)) and ‘peak-to-peak,’ according to the extended Giaever model (hereinafter referred to as the ‘single-hump model’), when it is assumed that the density of states (DOS) has a hump below E_F . This is consistent with the ARPES observations. From the SIS tunneling spectrum, the intrinsic hump and peak energies (E_H^* and E_P^*) in the DOS were calculated as $|E_H^{SIS} - E_P^{SIS}|/2$ (Fig. 1(b)) and $|E_P^{SIS}|/2$, respectively. Here, E_H^{SIS} and E_P^{SIS} are the visible hump and peak energies in the SIS tunneling spectrum, respectively. The visible hump and peak energies (E_H^{SIN} and E_P^{SIN}) in the SIN tunneling spectrum correspond to E_H^* and E_P^* , respectively (Fig. 1(a)). The visible hump and peak energies (E_H^{PES} and E_P^{PES}) in the ARPES EDC correspond to E_H^* and E_P^* , respectively.

Purely oxygen-doped $\text{Bi}_2\text{Sr}_2\text{CaCu}_2\text{O}_{8+\delta}$ (OD-Bi2212) is a popular HTCS because it is easy to obtain a clean and shiny surface parallel to the CuO_2 plane (or a - b plane) by cleavage at room temperature (RT) and ambient pressure. In 1995, Hancotte *et al.* reported that the tunneling spectrum through the SIN junction (SIN J) between OD-Bi2212 and a normal metal depends on whether the surface of OD-Bi2212 is cleaved at 4.2 K or RT.¹⁵ Briefly, the SIN J fabricated at 4.2 K produced a symmetrical spectrum, whereas that fabricated at RT produces an asymmetrical spectrum. In 2010, Palczewski *et al.* reported that the ARPES EDC of OD-Bi2212

depended on the temperature and environmental pressure when the sample surface was cleaved.¹⁶ Specifically, the surface cleaved at a low temperature under ultrahigh vacuum (UHV) was stable until the temperature or pressure was increased. Accordingly, for OD-Bi2212, sample fabrication at 4.2 K and under UHV is effective for producing an ideal junction or surface. This finding, as suggested by Ref.15, highlights the importance of the sample preparation conditions, a factor not previously emphasized in electronic phase diagrams, such as the UEPD established in 2008.¹³

Hancotte *et al.* also observed another symmetrical hump structure outside the symmetrical PDH structure in the tunneling spectrum through an SIS break junction (BJ) fabricated at 4.2 K.¹⁷ Unfortunately, the second symmetrical hump structure could not be explained by the previously mentioned single-hump model. According to Mourachkine's interpretation,¹⁸ the second symmetrical hump structure can be generated by a 'hump-to-hump' tunneling process (Fig. 1(d)) when the DOS has one pair of hump structures outside the paired peak structure (hereinafter referred to as the 'twin-hump model'). Thus, E_H^* can be calculated as $|E_{H2}^{SIS}|/2$ from the second hump peak (Fig. 1(d)), where E_{H2}^{SIS} is the peak energy of the second hump structure. E_H^* can also be calculated as $|E_H^{SIS}-E_P^{SIS}/2|$ (Fig. 1(c)). Fortunately, the relationship $E_H^* = |E_H^{SIS}-E_P^{SIS}/2|$ is independent of whether the hump-to-peak process is based on the single-hump model (Fig. 1(b)) or the twin-hump model (Fig. 1(c)). Accordingly,

the data from tunneling and photoemission spectroscopic measurements in UEPD should be re-examined only in terms of ‘sample fabrication conditions.’

In this study, the doping-induced evolution of E_H^* , as observed by tunneling or photoemission spectroscopic measurements in OD-Bi2212, was found to be significantly dependent on the sample fabrication conditions. When the samples were fabricated at 4.2 K and/or under UHV, E_H^* exhibited a step-like doping dependence. Furthermore, the intrinsic dip energy (E_D^*) corresponds to the upper PG line. However, as the fabrication conditions become poor, E_H^* and E_D^* reproduce previous results. Based on the observed effects of the sample fabrication conditions, it can be concluded that the observed results in the samples fabricated at 4.2 K and/or under UHV reflect an intrinsic bulk property, whereas the previous results reflect degraded surface properties. The dip energy can be considered as the boundary between the hump and peak contributions, although it is highly sensitive to sample fabrication conditions.

2. Method

The analyzed data for tunneling spectroscopy and ARPES were extracted from raw spectra^{3-12,17-20,31} and raw EDC along the antinodal direction^{21-30,32}, respectively, as reported in the literature. The sample fabrication conditions were determined from

literature, as discussed below. The broad hump structure is sometimes flat. If it is difficult to determine the visible hump energy from the published figures, the flat region and center position are shown using error bars and symbols, respectively. The doped-hole concentration (P_{pl}) should be determined according to the hole scale based on the thermoelectric power at 290 K, as reported by Honma and Hor (P_{pl} -scale).^{13,33} Unfortunately, the thermoelectric power was not accompanied by tunneling or ARPES data. Therefore, P_{pl} was estimated by comparing the T_c value in the literature with the half-dome-shaped T_c -curve of OD-Bi2212 in Ref.13, because T_c was provided along with its maximum value (T_c^{max}). In the case where T_c^{max} was not provided, 93 K was used as T_c^{max} . The method for estimating P_{pl} is provided in Ref.34. Information on the half-dome-shaped T_c -curve for OD-Bi2212 and some data points are available in Supplementary Material.

3. Results

Figure 2 shows the P_{pl} -dependencies of E_{H}^* and E_{P}^* with respect to sample fabrication conditions. E_{H}^* is significantly dependent on the sample fabrication conditions, whereas E_{P}^* is independent. The data plotted in Fig. 2(a) are from the tunneling spectra obtained at 4.2 and 6-7 K for SIS BJJs fabricated at 4.2^{6,9-12,17-19} and approximately 10 K,²² respectively. The details of these junctions are discussed later

in this study. Note that E_H^* does not follow the previous smooth doping dependence but follows a new step-like one. The step-like hump line exhibits four rapid descents at $P_{pl} \approx 0.17, 0.19, 0.27,$ and 0.28 with three plateaus between two adjacent descents. E_H^* was calculated as $|E_H^{SIS} - E_P^{SIS}/2|$ or $|E_{H2}^{SIS}|/2$. E_P^* ($=|E_P^{SIS}|/2$) lies on the previous lower PG line within the error band,¹³ although it appears to contain small structures. The tunneling data in Fig. 2(b) were obtained from the spectra at 4.2 K through SIN Js fabricated at 4.2 K^{6,7} or RT under UHV.^{3,4,8} The ARPES data in Fig. 2(b) were obtained from the EDC at 10-22 K from a surface cleaved under UHV.²¹⁻²⁵ $|E_H^{SIN}|$ and $|E_H^{PES}|$ follow the step-like hump line shown in Fig. 2(a), although $|E_H^{PES}|$ exhibits a slight downward deviation at $0.19 < P_{pl} < 0.24$. The data in Fig. 2(c) are obtained from the spectra at 4.2-8 K through SIN Js fabricated at RT in a He atmosphere⁵ and the ARPES EDC at 14-49 K on the cleaved surface obtained without special care.^{26,27} $|E_H^{SIN}|$ and $|E_H^{PES}|$ reproduce the previous smooth hump line in the UEPD.

The dip energy can also be classified based on sample fabrication conditions. In Figs. 3(a), 3(b), and 3(c), E_D^* is plotted as a function of P_{pl} using the same dataset as in Figs. 2(a), 2(b), and 2(c), respectively. E_D^{SIS} , E_D^{SIN} , and E_D^{PES} are the dip energies in the SIS tunneling spectrum, SIN tunneling spectrum, and ARPES EDC, respectively. Figure 3(a) shows the P_{pl} -dependence of $|E_D^{SIS}|/2$ from the SIS BJ fabricated at 4.2 and approximately 10 K. $|E_D^{SIS}|/2$ lies on the upper PG line at $P_{pl} <$

0.20, although it has a small upward bulge-like deviation from the upper PG line at $0.22 < P_{\text{pl}} < 0.28$. Figure 3(b) shows the P_{pl} -dependence of $|E_{\text{D}}^{\text{SIN}}|$ and $|E_{\text{D}}^{\text{PES}}|$ from the SIN J fabricated at 4.2 K or RT under UHV, and the surface cleaved under UHV. Although both $|E_{\text{D}}^{\text{SIN}}|$ and $|E_{\text{D}}^{\text{PES}}|$ follow the upper PG line at $P_{\text{pl}} < 0.18$, they deviate upward from the upper PG line at $P_{\text{pl}} > 0.18$. The bulge-like deviation appears to grow toward the high-energy side. At $0.16 < P_{\text{pl}} < 0.20$, $|E_{\text{D}}^{\text{SIN}}|$ is slightly larger than $|E_{\text{D}}^{\text{PES}}|$. This may be because of the broad hump structure of the SIN spectrum. As shown in Fig. 2(b), the plotted $|E_{\text{H}}^{\text{SIN}}|$ data points have relatively longer error bars. Figure 3(c) shows the P_{pl} -dependence of $|E_{\text{D}}^{\text{SIN}}|$ and $|E_{\text{D}}^{\text{PES}}|$ for the SIN J fabricated at RT in He atmosphere or the cleaved surface without special care. The bulge was the largest. The bulge-like deviation seems to grow with deterioration of the sample fabrication conditions. Thus, the dip energy is highly sensitive to the sample fabrication conditions.

Figure 4 shows the P_{pl} -dependence of the PG temperature (T^*) and other related temperatures obtained using experimental spectroscopic probes.^{12,20,21,23,26,28-32} In Fig. 4(a), all the plotted T^* values follow the upper PG line, although there is some scattering. The energy resolution of the ARPES data in Fig. 4(a) is less than 8 meV^{23,30} for half-black symbols and greater than 15 meV^{26,28,29} for red symbols, and the energy resolution of the tunneling data is greater than 1 meV.⁵ Accordingly, the T^* values distributed between the upper and lower PG lines are considered to result

from a relatively low energy resolution. Because the dip and peak energies follow the upper and lower PG lines, respectively, the peak structure appears at the upper PG line or T^* . In Fig. 4(b), the pair formation temperature (T_{c0}) of intrinsic Josephson junctions (IJJs)³¹ follows the lower PG line. Another PG temperature (T_0), referred to as the large PG temperature, was observed using angle-integrated photoemission spectroscopy.²³ T_0 was on the smooth hump line. T^* and pair formation temperature (T_{pair}) of ARPES³² followed the smooth hump and upper PG lines, respectively. Thus, the other reported characteristic temperatures observed by the experimental spectroscopic probes follow either the hump, upper PG, or lower PG lines, although we do not know why T^* in Ref.32 follows the hump line rather than the upper PG line.

4. Discussion

The SIS BJs of the samples plotted in Figs. 2(a) and 3(a) were fabricated at 4.2 or approximately 10 K using the scanning tunneling microscope (STM) technique (or the point-contact technique; PCT) or the conventional BJ technique. In the STM technique, the SIS BJ is formed by perforating the cleaved topmost layer by pushing the metal tip along the c -axis to the surface of the OD-Bi2212.^{5,7} According to Ozyuzer's interpretation,⁷ the insulator layer of the SIS BJ consists of adjacent Bi-O insulator layers, such as IJJs.³¹ In the conventional BJ technique, the junction is

formed by bending along the a - b plane at 4.2 K in a He atmosphere.^{11,17} Neither of the tunneling currents passed through the topmost layer after cleavage. Thus, the SIS tunneling spectra through the SIS BJ fabricated at 4.2 or 10 K are relatively free from degradation caused by the cleaving process. Under these conditions, the probes can detect a pure virgin surface property, that is, the intrinsic bulk property. The SIN Js of the samples plotted in Figs. 2(b) and 3(b) were fabricated at 4.2 K or RT under UHV, and the surfaces of the samples for ARPES plotted in Figs. 2(b) and 3(b) were cleaved under UHV. Using the STM technique, a SIN J was formed by adjusting the pushing pressure of the tip against the cleaved surface.^{7,35} A sufficiently high pressure formed the SIS BJ. However, when the pressure is either too low or too high, the junction does not function. A moderate pressure is required to form SIN J. Accordingly, the fabrication of SIN J may be more challenging than that of SIS BJ. Although cleavage under UHV can decrease the possibility of contamination by surface exposure,¹⁶ this risk remains. This explains the slight downward deviation of $|E_H^{\text{PES}}|$ from the step-like doping dependence shown in Fig. 2(b). The SIN Js formed by the STM technique (or PCT) in Figs. 2(c) and 3(c) were fabricated at RT in He atmosphere. According to Ref.15, the junctions fabricated at RT are unstable. When the surface of the sample for ARPES measurement is cleaved without special care, it becomes unstable.¹⁶ Thus, the tunneling currents pass through the degraded junction, and the photoelectrons are picked up from the surface degraded by

cleavage. Under these conditions, the probes could detect the properties of the degraded surface. Therefore, the step-like hump behavior shown in Fig. 2(a) is a bulk property, whereas the smooth hump behavior shown in Fig. 2(c) reflects the properties of a degraded surface.

As shown in Fig. 3, a bulge-like deviation in the dip energy was produced by the broadening of the hump and peak structures. Because the sharp peak had a higher intensity than the broad hump, the broadening effect of the peak was larger than that of the hump. Consequently, the bulge always grows toward the high-energy side because of broadening from degradation during sample fabrication. When UEPD was established, the dip energy did not follow any lines in the UEPD. This issue originates from the sample fabrication problems. In Fig. 3, a lower energy resolution results in a larger scattering. However, this influence did not directly contribute to the broadening effect. Poor sample fabrication conditions prevented the identification of the intrinsic behavior of dip energy, particularly on the overdoped side. On the overdoped side, the peak energy is closer to the hump energy, causing a partial overlap. The dip energy depends on the degree of this overlap, resulting in a small bulge-like deviation at $0.22 < P_{pl} < 0.28$ in Fig. 3(a). This deviation was enhanced by the deterioration of the sample fabrication conditions. Therefore, the dip energy following the upper PG line was an intrinsic property.

As shown in Fig. 4, T^* values observed by the spectroscopic probes follow the upper PG line. The PG temperature was reported as a downward deviation from the T -linear dependence of the in-plane resistivity.³⁶ The resistive T^* also follows the upper PG¹³. Accordingly, the resistive downward deviation at T^* can be related to the growth of the peak structure, that is, the enhancement of the DOS.

The three hump, upper PG, and lower PG lines in the previous UEPD were extracted from various characteristic energies/temperatures observed by different probes and groups.¹³ Unfortunately, no single experimental probe detected all three energies (hump, upper PG, and lower PG), although some probes detected only one or two energies. This study revealed that this problem stems from the sample fabrication issues. The hump, dip, and peak energies observed in the samples fabricated at 4.2 K and/or under UHV by tunneling and ARPES measurements correspond to the hump, upper PG, and lower PG energies in the UEPD, respectively.

The peak energy follows the lower PG line of the previous UEPD.¹³ In the samples fabricated at 4.2 K, the intrinsic peak energy ($|E_P^{\text{SIS}}|/2$), which belongs to the lower PG, exhibited a minor structure, although it was buried in the error band of the lower PG line.¹³ This structure appears to be related to the step-like hump behavior; however, it is challenging to check small structures because of resolution issues.

The application of the P_{pl} -scale extracted a step-like doping dependence of T_c , which has three T_c jumps at $P_{pl} = P_4, 2P_4,$ and $3P_4$, in purely oxygen-doped $\text{YBa}_2\text{Cu}_3\text{O}_{6+\delta}$ ³⁷ and $\text{La}_2\text{CuO}_{4+\delta}$ ³⁸ from the oxygen-content (δ) dependency of T_c . Here, P_4 is equal to $1/16$ based on 4×4 charge ordering. In the oxygen and cation co-doped $\text{Bi}_2\text{Sr}_{2-x}\text{La}_x\text{CuO}_{6+\delta}$, the insulator-superconductor (IS) transition appears at $P_{pl} \approx 0.11 \approx P_3$.³³ Here, P_3 is equal to $1/9$ based on 3×3 charge ordering.³⁷ In OD-Bi2212, the P_{pl} -dependency of E_H^* exhibits four rapid descents at $P_{pl} \approx 0.17, 0.19, 0.27,$ and 0.28 . $P_{pl} \approx 0.17, 0.19, 0.27,$ and 0.28 are corresponding to $1/6, 3/16, 77/288,$ and $9/32$, respectively. Based on the hierarchical behavior, the P_{pl} values of $1/6, 3/16, 77/288,$ and $9/32$ can be represented as $(P_3+2P_3)/2 = 1.5P_3, 3P_4, (2P_3+5P_4)/2,$ and $(4P_4+5P_4)/2 = 4.5P_4$, respectively. In the half-dome-shaped T_c -curve of OD-Bi2212 (red broken line in Figs. 2 and 3),¹³ IS transition, T_c^{\max} , and T_c disappearance occur at $P_{pl} \approx 0.09, 0.24,$ and 0.31 , corresponding to $3/32, 17/72,$ and $5/16$, respectively. The values of $P_{pl} = 3/32, 17/72,$ and $5/16$ can be represented by $(P_4+2P_4)/2 = 1.5P_4, (2P_3+4P_4)/2,$ and $5P_4$, respectively. Thus, the characteristic features of OD-Bi2212 appear in a hierarchical order based on P_4 and the mixing level of the nearest P_4 or P_3 . Although OD-Bi2212 is a purely oxygen-doped HTCS, it has an incommensurate superlattice structure along the b -axis.³⁹ The superlattice structure may influence this hierarchical order.

5. Conclusion

The doping-induced evolution of E_H^* and E_D^* , as extracted from the tunneling spectra or ARPES EDC of OD-Bi2212, was studied in terms of sample fabrication conditions. E_H^* exhibited step-like doping dependence when the samples were fabricated at 4.2 K and/or under UHV conditions. E_D^* follows the upper PG line. However, as the fabrication conditions deteriorated, the doping dependence of E_H^* and E_D^* reproduced the previous behavior. Therefore, it can be concluded that E_H^* and E_D^* of the samples fabricated at 4.2 K and/or under UHV conditions reflect the bulk properties, whereas those of the samples fabricated under poor conditions reflect degraded surface properties. Unfortunately, the bulk property cannot be resolved against the intrinsic peak energy because of the resolution limitations of experimental probes. Therefore, a special analytical technique is required to identify intrinsic features from extensive and reliable data on OD-Bi2212. This study is currently in progress.

Acknowledgements

The author appreciates the collaboration with Dr. Pei-Herng Hor (Department of Physics and Texas CTR for Superconductivity at the University of Houston) for over 20 years. Unfortunately, he passed away in the early spring of 2021.

References

1. Dessau D S, Wells B O, Shen Z -X, Spicer, A. J. Arko, List E S, Mitzi D B and Kapitulnik A 1991 *Phys. Rev. Lett.* **66**, 2160-2163
2. Huang Q, Zasadzinski J F, Gray K E, Liu J Z and Claus H 1989 *Phys. Rev. B* **40**, 9366R
3. Renner Ch and Fischer Ø 1995 *Phys. Rev. B* **51**, 9208-9218
4. Renner Ch, Revaz B, Genoud J -Y, Kadowaki K and Fischer Ø 1998 *Phys. Rev. Lett.* **80**, 149-152
5. DeWilde Y, Miyakawa N, Guptasarma P, Iavaroune M, Ozyuzer L, Zasadzinski J F, Romano P, Hinks D G, Kendziora C, Crabtree G W and Gray K E 1998 *Phys. Rev. Lett.* **80**, 153-156
6. Miyakawa N, Zasadzinski J F, Ozyuzer L, Guptasarma P, Hinks D G and Kendziora C 1999 *Phys. Rev. Lett.* **83**, 1018-1021
7. Ozyuzer L, Zasadzinski J F, Kendziora C, Gray K E 2000 *Phys. Rev. B* **61**, 3629-3640
8. Fang A, Howald C, Kaneko N, Greven M and Kapitulnik A 2004 *Phys. Rev. B* **70**, 214514

9. Ozyuzer L, Zasadzinski J F and Miyakawa N 1999 *Int. J. Mod. Phys. B* **29-31**, 3721-3724
10. Zasadzinski J F, Ozyuzer L, Miyakawa N, Gray K E, Hinks D G, and Kendziora C 2001 *Phys. Rev. Lett.* **87**, 067005
11. Mourachkine A 2001 *Europhys. Lett.* **55**, 559-565
12. Ozyuzer L, Zasadzinski J F, Gray K E, Kendziora C and Miyakawa N 2002 *Europhys. Lett.* **58**, 589-595
13. Honma T and Hor P H 2008 *Phys. Rev. B* **77**, 184520
14. Giaever I, Megerle K 1961 *Phys. Rev.* **122**, 1101-1111
15. Hancotte H, Davydov D N, Ye M and Deltour R 1995 *Physica B* **204**, 206-213
16. Palczewski A D, Kondo T, Wen J S, Xu G Z J, Gu G and A. Kaminski A 2010 *Phys. Rev. B* **81**, 104521
17. Hancotte H, Davydov D N, Deltour R, Jansen A G M and Wyder P 1997 *Physica C* **280**, 71-76.
18. Mourachkine A 2005 *Mod. Phys. Lett. B* **19**, 743-770
19. Vedeneev S I, Jansen A G M, Samuely P, Stepanov V A, Tsvetkov A A and Wyder P 1994 *Phys. Rev. B* **49**, 9823-9830

20. Dipasupil R M, Oda M, Momono N and Ido M 2002 *J. Phys. Soc. Jpn.* **71**, 1535-1540
21. Sun X, Zhang W -T, Zhao L, Liu G -D, Yang F, Chen C -T, Xu Z -Y and Zhou X -J 2018 *Chin. Phys. Lett.* **35** 017401
22. Ai P, Gao Q, Liu J, Zhang Y, Li C, Huang J, Song C, Yan H, Zhao L, Liu G, Gu G, Zhang F, Yang F, Peng Q, Xu Z and Zhou X J 2019 *Chin. Phys. Lett.* **36**, 067402
23. Takahashi T, Sato T, Yokoya T, Kamiyama T, Naitoh Y, Mochiku T, Yamada K, Endoh Y, Kadowaki K 2001 *J. Phys. Chem. Solids* **62**, 41-45
24. Lee W S, Vishik I M, Tanaka K, Lu D H, Sasagawa T, Hagaosa N, Devereaux T P, Hussian Z and Shen Z -X 2007 *Nature (London)* **450** 81
25. Vishik I M, Nowadnick E A, Lee W S, Shen Z X, Moritz, Devereaux T P, Tanaka K, Sasagawa T and Fujii T 2009 *Nat. Phys.* **5**, 718-721
26. Campuzano J C, Ding H, Norman M R, Fretwell H M, Randeria M, Kaminski A, Mesot J, Takeuchi T, Sato T, Yokoya T, Takahashi T, Mochiku T, Kadowaki K, Guptasarma P, Hinks D G Konstantinovic Z, Li Z Z and H. Raffy H 1999 *Phys. Rev. Lett.* **83**, 3709-3712

27. Ding H, Engelbrecht J R, Wang Z, Campuzano J C, Wang S -C, Yang H -B, Rogan R, Takahashi T, Kadowaki K and Hinks D G 2001 *Phys. Rev. Lett.* **87**, 227001
28. Chatterjee U, Ai D, Zhao J, Rosenkranz S, Kaminski A, Raffy H, Li Z, Kadowaki K, Randeria M, Norman M R and Campuzano J C 2011 *Proc. Natl. Acad. Sci.* **108**, 9346-9349
29. Ding H, Yokoya T, Campuzano J C, Takahashi T, Randeria M, Norman M R, Mochiku T, Kadowaki K and Giapintzakis J 1996 *Nature (London)* **382** 51
30. Vishik I M, Hashimoto M, He R -H Lee W -S, Schmitt F, Lu D, Moore R G, Zhang C, Meevasana W, Sasagawa T, Uchida S, Fujita K, Ishida S, Ishikado M, Yoshida Y, Eisaki H, Hussain Z, Devereaux T P, Shen Z -X 2012 *Proc. Natl. Acad. Sci.* **109**, 18332-18337
31. Ren J K, Zhu X B, Yu H F, Tian Y, Yang H F, Gu C Z, Wang N L, Ren Y F and Zhao S P 2012 *Sci. Rep.* **2**, 248
32. Kondo T, Palczewski A D, Hamaya Y, Takeuchi T, Wen J S, Xu Z J, Gu G and Kaminski A 2013 *Phys. Rev. Lett.* **111**, 157003
33. Honma T, Hor P H, Hsieh H H and Tanimoto M 2004 *Phys. Rev. B* **70**, 214517
34. Honma T and Hor P H 2015 *Int. J. Mod. Phys. B* **29**, 1542029

35. Fischer Ø, Kugler M, Maggio-Aprile I, Berthod C and Renner Ch 2007 *Rev. Mod. Phys.* **79**, 353
36. Ito T, Takenaka K and Uchida S 1993 *Phys. Rev. Lett.* **70**, 3995
37. Honma T and Hor P H 2007 *Phys. Rev. B* **75**, 012508
38. Kim Y H, Song Y S and Hor P H 2012 *Mod. Phys. Lett. B* **26**, 1150020
39. Matsui Y, Maeda H, Tanaka Y and Horiuchi S 1988 *Jpn. J. Appl. Phys.* **27**, L372

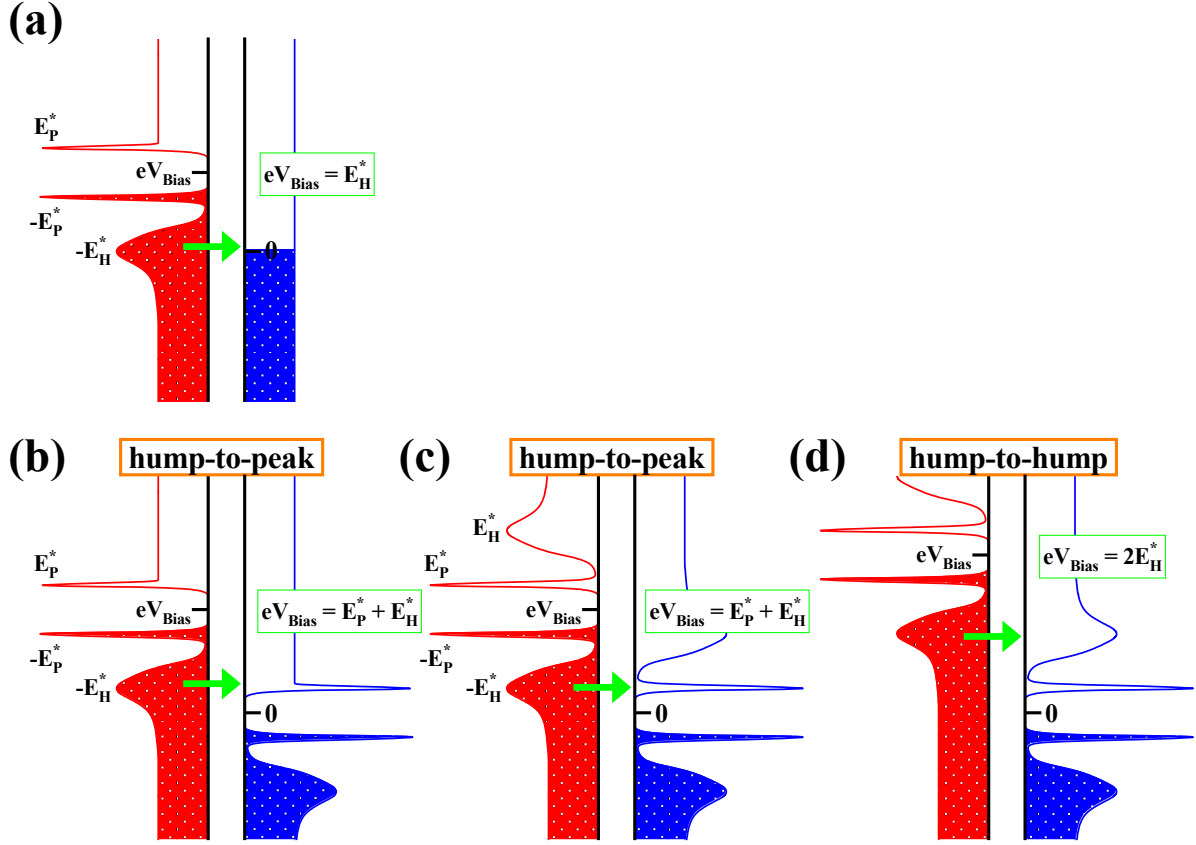


Figure 1. (Color online) Schematic of the SIN or SIS tunneling related to the hump energy of the HTCS at 0 K (based on Refs.14 and 18). (a) SIN tunneling with $V_{\text{Bias}} = E_H^*/e$ (single-hump). (b) SIS tunneling with $V_{\text{Bias}} = (E_H^* + E_P^*)/e$ (single-hump). (c) SIS tunneling with $V_{\text{Bias}} = (E_H^* + E_P^*)/e$ (twin-hump). (d) SIS tunneling with $V_{\text{Bias}} = 2E_H^*/e$ (twin-hump). V_{Bias} and e are the bias voltage and electron charge, respectively. The thick arrows show the main tunneling process.

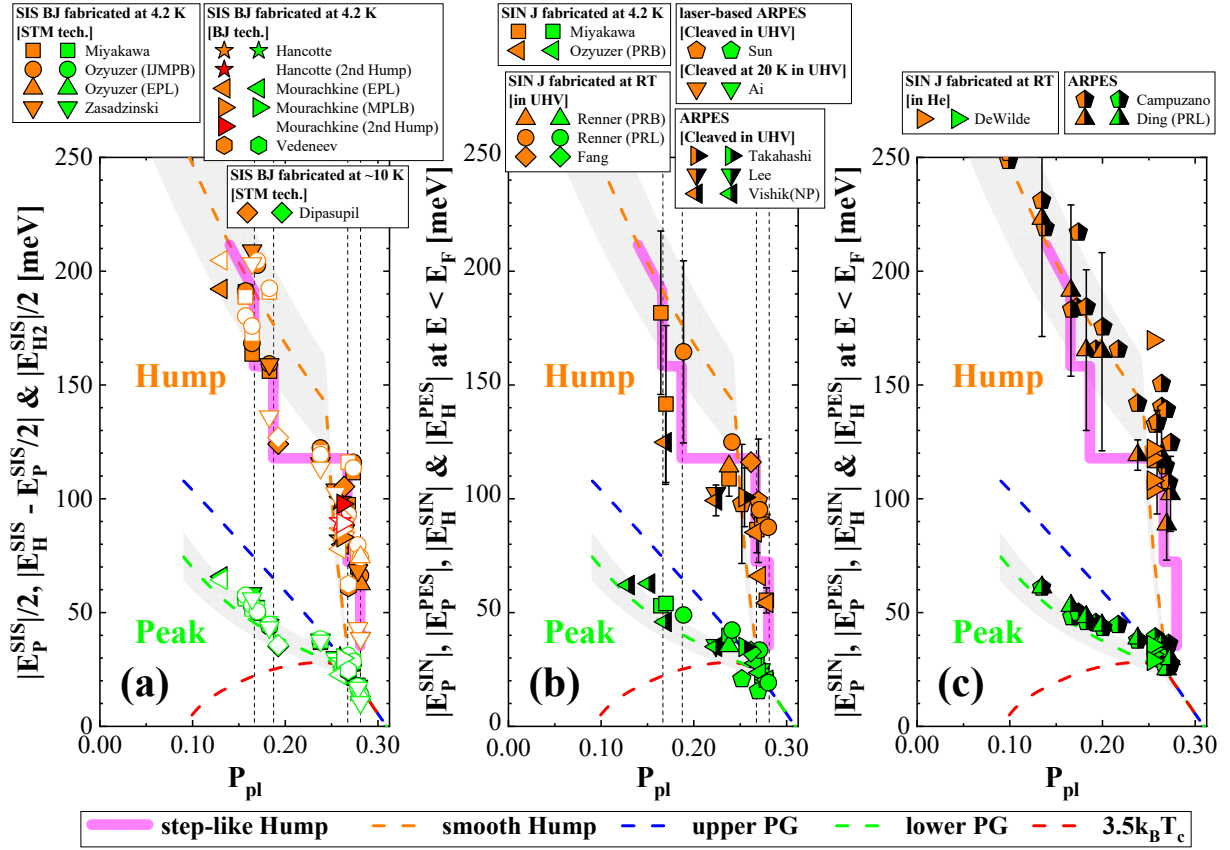


Figure 2. (Color online) P_{pl} -dependencies of E_H^* and E_P^* extracted from the tunneling spectra and ARPES EDC. (a) Based on the spectrum through the SIS BJ fabricated at 4.2 K^{6, 9-12, 17-19} and approximately 10 K.²⁰ Red symbols show $|E_{H2}^{SIS}|/2$. Closed and open symbols show the data at $E < E_F$ and $E > E_F$, respectively. (b) Based on the spectrum through the SIN J fabricated at 4.2 K^{6,7} and at RT under UHV,^{3,4,8} and the EDC from the surface cleaved under UHV.²¹⁻²⁵ (c) Based on the spectrum through the SIN J fabricated at RT in He atmosphere⁵ and the EDC from the surface cleaved at RT.²⁶⁻²⁸ Orange and green symbols show the hump and peak energies, respectively. The energy resolution of ARPES is below 8 meV²³⁻²⁵ in Fig. 2(b) and over 15 meV^{26,27} in Fig. 2(c). The energy resolution of the tunneling⁵ and laser-based ARPES^{21,22} is 1 meV.

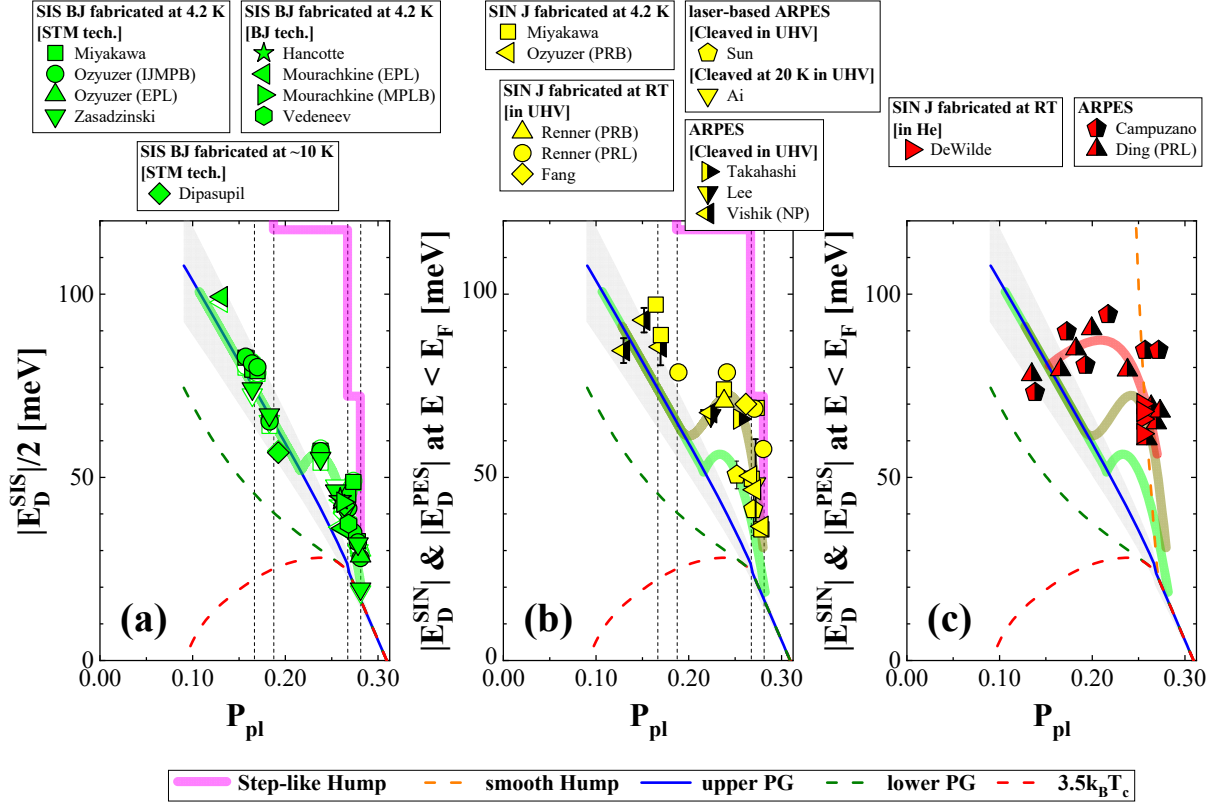


Figure 3. (Color online) P_{pl} -dependence of E_D^* . (a) Based on the same dataset in Fig. 2(a). Because the dip energy at $E < E_F$ is almost equal to that at $E > E_F$, both symbols are almost overlapped. (b) Based on the same dataset in Fig. 2(b). Half-black symbols show the dip energy, having an energy resolution of 7-8 meV. (c) Based on the same dataset in Fig. 2(c).

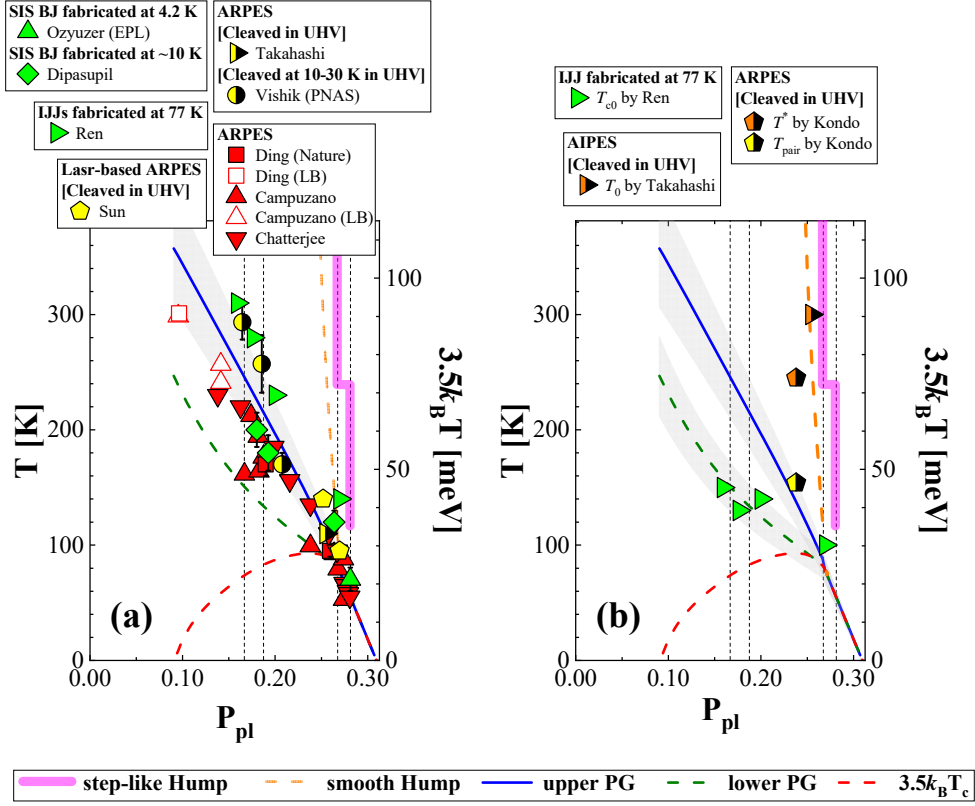


Figure 4. (Color online) P_{pl} -dependence of T^* and the other related temperature. (a) P_{pl} -dependence of T^* . T^* values are from SIS tunneling,^{12,20} laser-based ARPES,²¹ ARPES,^{23,26,28-30} and IJJs.³¹ The energy resolution of ARPES is below 8 meV for the half-black symbols^{23, 25} and over 15 meV for the red symbols.^{26,28,29} The energy resolution of the tunneling⁵ and laser-based ARPES²¹ is 1 meV. (b) P_{pl} -dependence of the other related temperature. T_0 and T_{c0} are from AIPES²³ and IJJs,³¹ respectively. T^* and T_{pair} by ARPES.³² The temperature (T) scale and energy (E) scale are related by $E = 3.5k_B T$,¹³ where k_B is the Boltzmann constant. The open symbols show the lower bounds (LB) for T^* .^{26,29} The energy resolutions of ARPES and AIPES are 10³² and 7 meV,²³ respectively.

**Supplementary Material for the doping-induced evolution of the
intrinsic hump and dip energies dependent on the sample fabrication
conditions in $\text{Bi}_2\text{Sr}_2\text{CaCu}_2\text{O}_{8+\delta}$**

Tatsuya Honma

Department of Physics, Asahikawa Medical University, Asahikawa 078-8510,
Japan

Determination of P_{pl}

A detailed description of P_{pl} was published by Honma and Hor [13,33,34]. The first and most reliable method for extracting P_{pl} is to determine the value of P_{pl} from the thermoelectric power at 290 K (S290) using P_{pl} -scale [13,30]. In the second method, P_{pl} is determined from T_c by comparison with a universal half-dome-shaped T_c -curve.¹³ The universal half-dome-shaped T_c -curve was based on P_{pl} determined from S290. The T_c -curve of OD-Bi2212 is shown in Fig. S1. The values of these data points are listed in Table S1. Unfortunately, in the present analysis, the value of S(290) is not available in the literature. Therefore, the determination of P_{pl} was based on a second method. The P_{pl} value was estimated from the T_c -curve shown in Fig. S1, after T_c of the samples was scaled by T_c^{\max} .

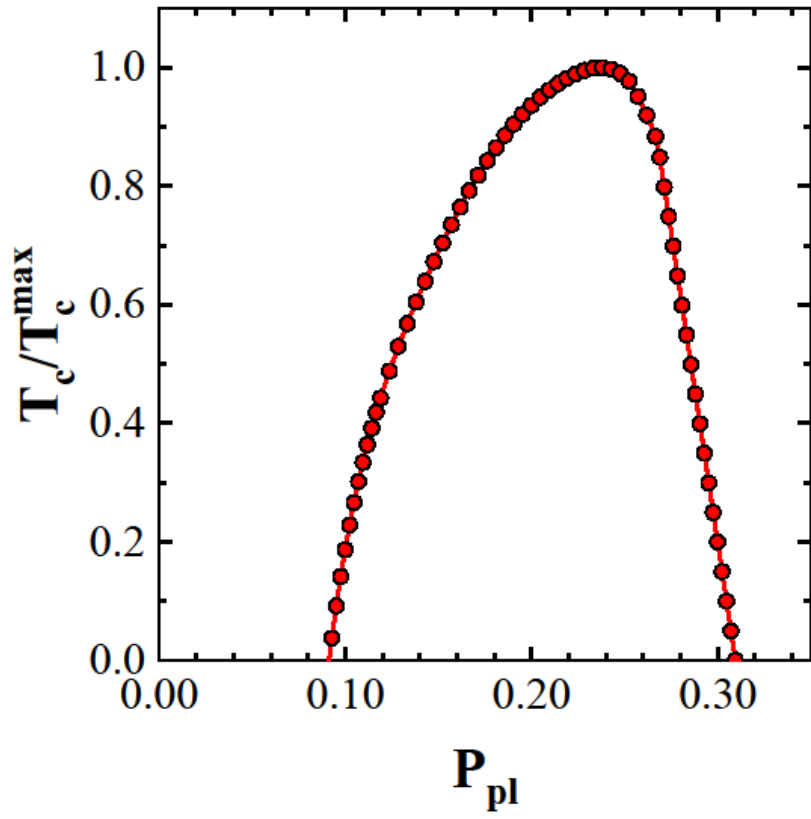


Fig. S1. (Color online) A half dome-shaped T_c -curve for $\text{Bi}_2\text{Sr}_2\text{CaCu}_2\text{O}_{8+\delta}$.¹³ The data for the red circles are listed in the table S1.

T_c/T_c^{\max}	P_{pl}
0.0375	0.0928
0.0918	0.0952
0.1413	0.0976
0.1867	0.1000
0.2282	0.1023
0.2663	0.1047
0.3014	0.1071
0.3339	0.1095
0.3639	0.1119
0.3919	0.1142
0.4181	0.1166
0.4428	0.1190
0.4882	0.1238
0.5296	0.1285
0.5681	0.1333
0.6044	0.1380
0.6390	0.1428
0.6723	0.1476
0.7043	0.1523
0.7350	0.1571

T_c/T_c^{\max}	P_{pl}
0.7643	0.1618
0.7921	0.1666
0.8182	0.1714
0.8426	0.1761
0.8651	0.1809
0.8856	0.1856
0.9043	0.1904
0.9212	0.1952
0.9364	0.1999
0.9499	0.2047
0.9620	0.2094
0.9726	0.2142
0.9818	0.2190
0.9895	0.2237
0.9953	0.2285
0.9990	0.2332
1.0000	0.2380
0.9974	0.2428
0.9903	0.2475
0.9774	0.2523

T_c/T_c^{\max}	P_{pl}
0.9513	0.2570
0.9196	0.2618
0.8837	0.2666
0.8485	0.2689
0.7986	0.2713
0.7486	0.2737
0.6987	0.2761
0.6488	0.2785
0.5989	0.2808
0.5490	0.2832
0.4991	0.2856
0.4492	0.2880
0.3993	0.2904
0.3494	0.2927
0.2995	0.2951
0.2495	0.2975
0.1996	0.2999
0.1497	0.3023
0.0998	0.3046
0.0499	0.3070

Table S1 Scaled T_c (T_c/T_c^{\max}) and the corresponding value of P_{pl} for the red circles plotted in Fig. S1.